Electronic Supplementary Material (ESI) for New Journal of Chemistry.

Supporting Information

Luminescent on-off probe based Calix[4]arene Linked through Triazole with Ruthenium (II) polypyridine complexes to Sense Copper (II) and Sulfide ions

Mohanraj Ramachandran [a], Sambandam Anandan*[a] and Muthupandian Ashokkumar[b]

[a]Department of Chemistry, National Institute of Technology, Tiruchirappalli 620 015, India

[b]School of Chemistry, University of Melbourne, Vic 3010, Australia

TABLE OF CONTENT

No.	Content	Fig. No.	Page. No.
1.	^{1}H NMR spectrum of **1** in $CdCl_3$	**Fig. S1**	4
2.	^{13}C NMR spectrum of **1** in $CdCl_3$	**Fig. S2**	4
3.	^{1}H NMR spectrum of **2a** in $CdCl_3$	**Fig. S3**	5
4.	^{13}C NMR spectrum of **2a** in $CdCl_3$	**Fig. S4**	5
5.	^{1}H NMR spectrum of **2b** in $CdCl_3$	**Fig. S5**	6
6.	^{13}C NMR spectrum of **2b** in $CdCl_3$	**Fig. S6**	6
7.	^{1}H NMR spectrum of **2c** in $CdCl_3$	**Fig. S7**	7
8.	^{13}C NMR spectrum of **2c** in $CdCl_3$	**Fig. S8**	7
9.	^{1}H NMR spectrum of **2d** in $CdCl_3$	**Fig. S9**	8
10.	^{13}C NMR spectrum of **2d** in $CdCl_3$	**Fig. S10**	8
11.	^{1}H NMR spectrum of **L** in $CdCl_3$	**Fig. S11**	9
12.	^{13}C NMR spectrum of **L** in $CdCl_3$	**Fig. S12**	9
13.	MALDI-TOF Mass spectrum of **L**	**Fig. S13**	10
14.	^{1}H NMR spectrum of **Ru_2L** in DMSO-d_6	**Fig. S14**	10
15.	^{13}C NMR spectrum of **Ru_2L** in DMSO-d_6	**Fig. S15**	11
16.	MALDI-TOF Mass spectrum of **Ru_2L**	**Fig. S16**	11
17.	FT-IR Spectra for Compound **1, 2d** (ATR Mode) and **L**	**Fig. S17**	12
18.	(A) UV-Vis and Fluorescence Spectrum of **Ru_2L**, (B) UV-Vis Spectra of **Ru_2L**, **Ru_2L+ Other metal ions** and **Ru_2L+Cu^{2+}**	**Fig. S18**	12
19.	(A) Under UV light illumination, **Ru_2L** with metal ions, (B) **Ru_2L+Cu^{2+}** with anions	**Fig. S19**	12
20.	(A) pH variation was monitored with **Ru_2L**, **Ru_2L-Cu^{2+}** and **Ru_2L-Cu^{2+}+S^{2-}** (B) **Ru_2L-Cu^{2+}** was examined in three different pH values with respect to time	**Fig. S20**	13
21.	EPR Spectra of **Ru_2L** and **Ru_2L+Cu^{2+}** at RT (A) and LNT (B)	**Fig. S21**	13
22.	(A) Cyclic Voltammetric diagram for **Ru_2L** and **Ru_2L-Cu^{2+}**, (B) Time decay profile diagram of **Ru_2L** and **Ru_2L-Cu^{2+}**	**Fig. S22**	13
23.	(A) Job's plot using the fluorescence intensity of **Ru_2L** and Cu^{2+}, (B) **Ru_2L** interaction with Cu^{2+} ion and then S^{2-} anion	**Fig. S23**	14

24.	(A) UV-Vis and (B) Fluorescence spectrum of Ru_2L, Ru_2L+Cu^+ in 10 μM CH_3CN/HEPES buffer (pH = 7.4) (8/2, v/v).	**Fig. S24**	14
25.	pH variation was checked to probe with other metal ions (10 equiv.) (Ru_2L+M), in addition of copper (II) ions (4 equiv.) to probe with other metal ions ($Ru_2L+M+Cu^{2+}$) (M = other metal ions).	**Fig. S25**	14
26.	Cytotoxic effect of the complex **Ru_2L** on A549 cells	**Fig. S26**	15
27.	(A) AO/EB staining indicating the percentage of A549 with **Ru_2L**, (B) Hoechst 33258 staining study of control and **Ru_2L** induced apoptosis of A549 cells. The graph is shown a manual count of apoptotic cells in percentage.	**Fig. S27**	15

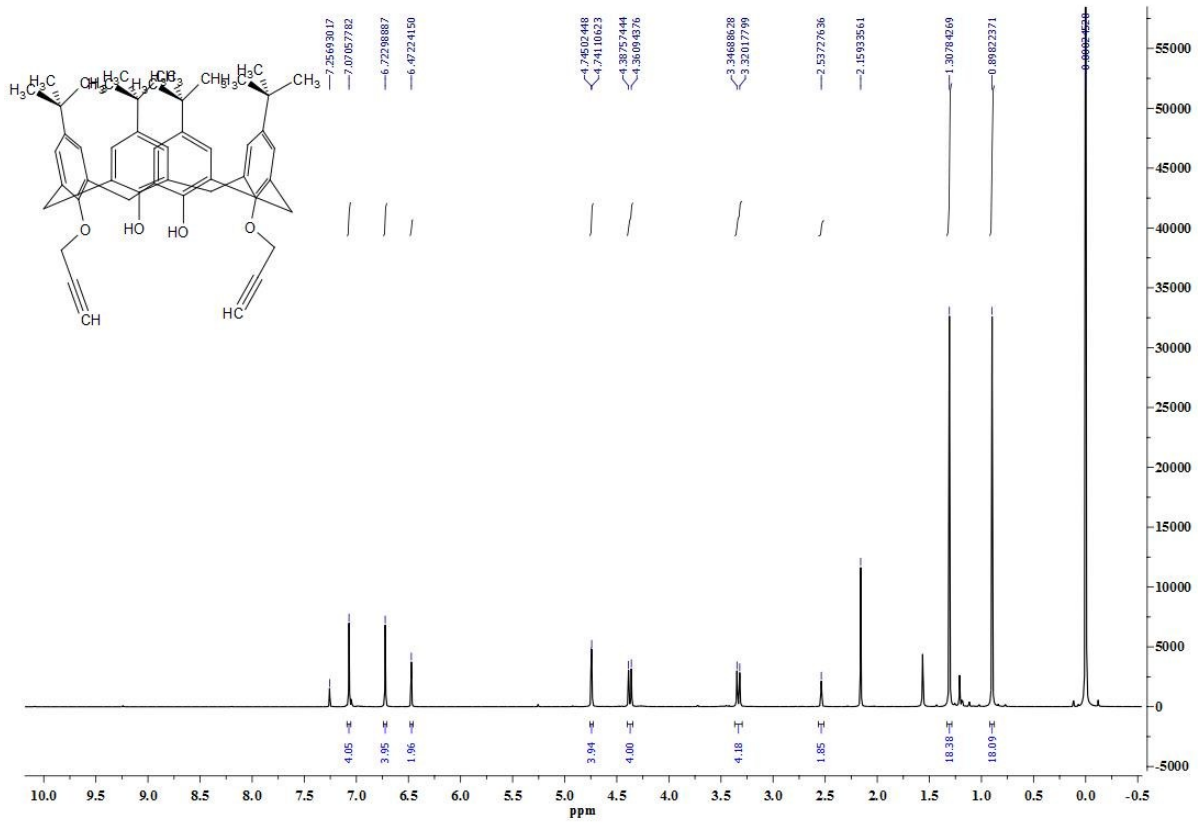

Fig. S1. ^{1}H NMR spectrum for 5,11,17,23-tetra-t-butyl-25,27-bis(O-propargyl)calix[4a]rene (**1**)

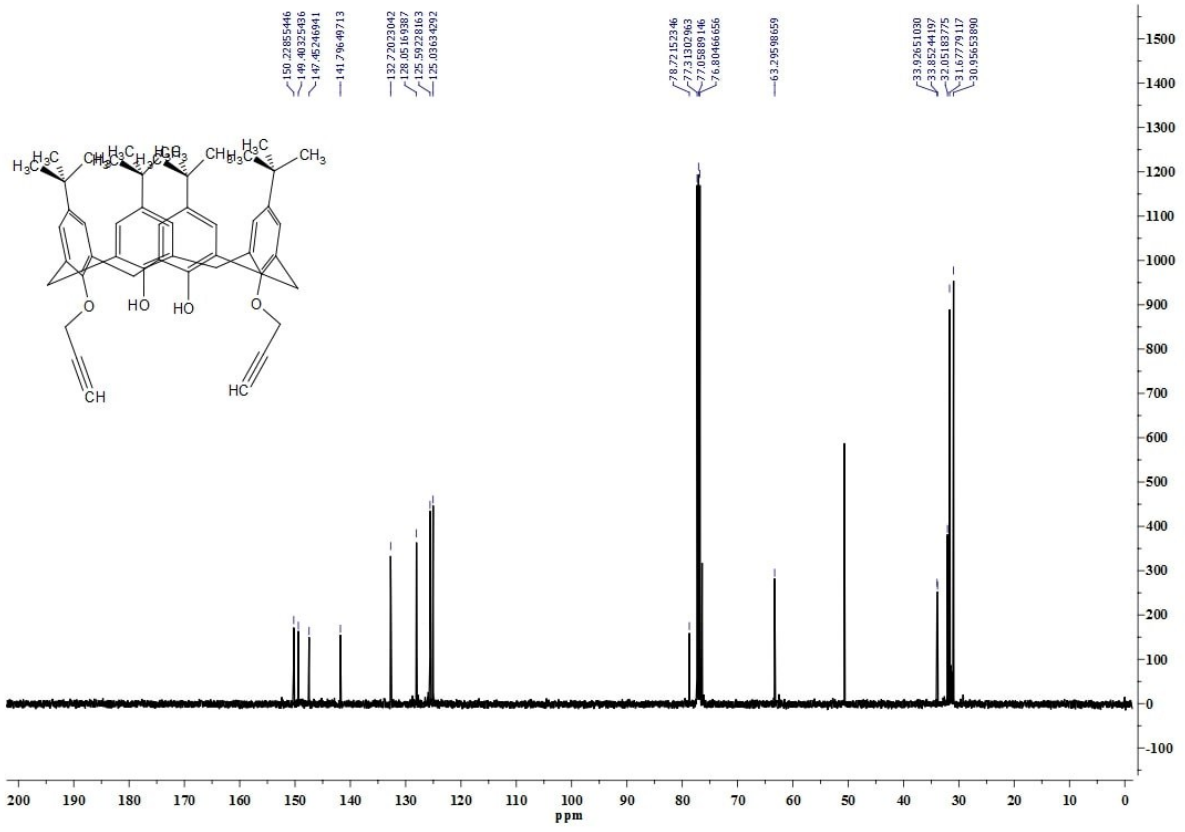

Fig. S2. ^{13}C NMR spectrum for 5,11,17,23-tetra-t-butyl-25,27-bis(O-propargyl)calix[4]arene (**1**)

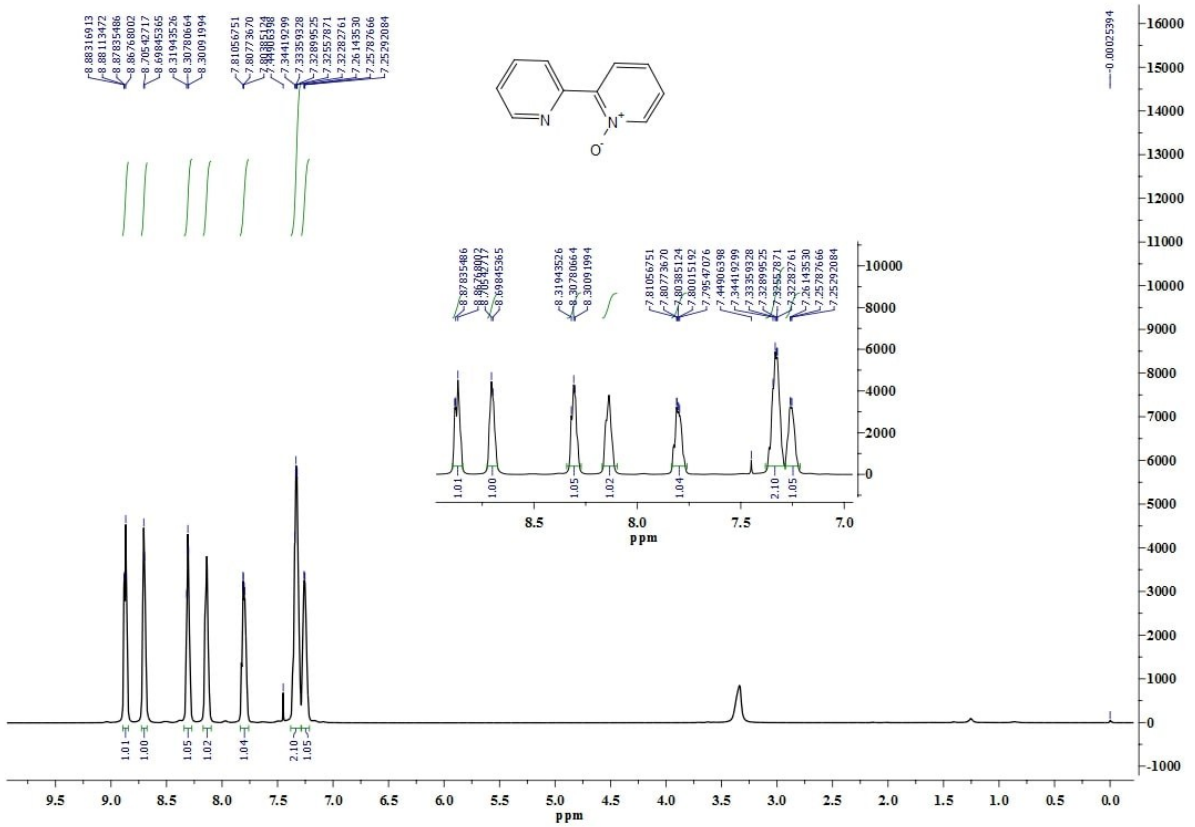

Fig. S3. ^{1}H NMR spectrum for 2,2-bipyridine-N-oxide (**2a**)

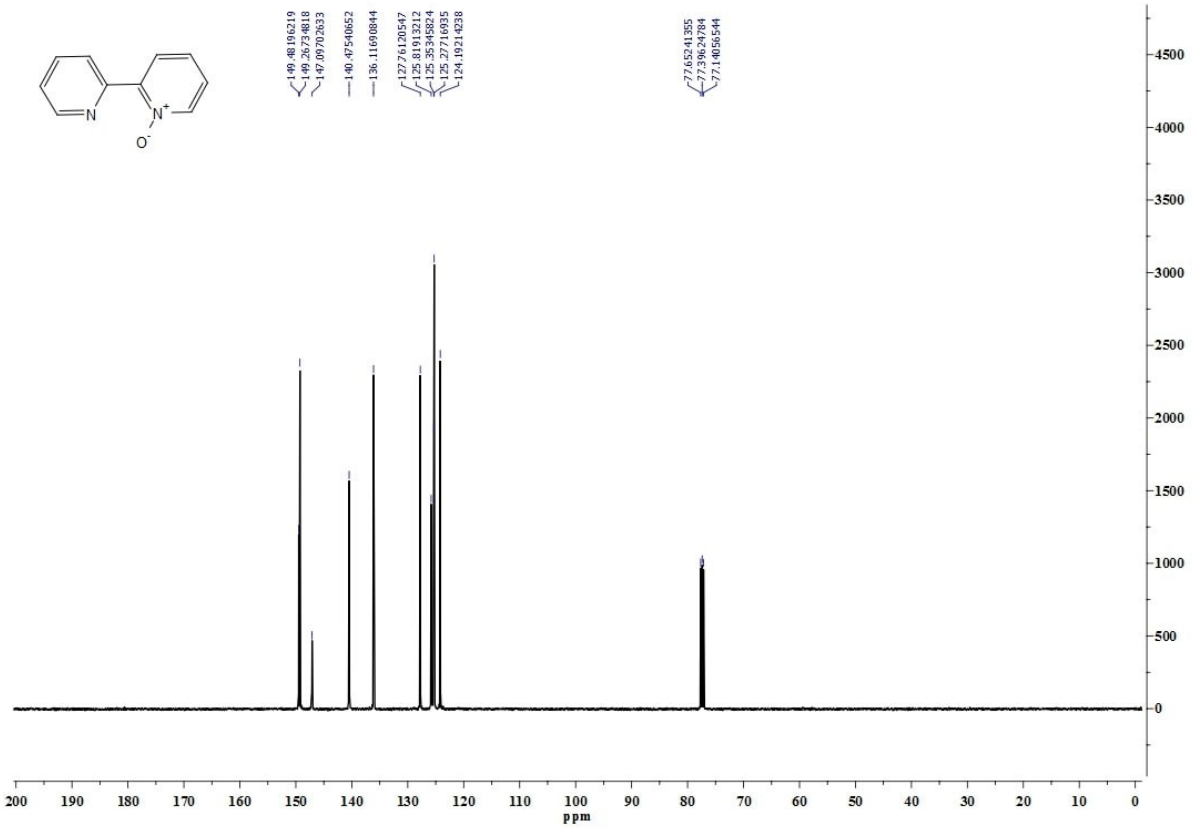

Fig. S4. ^{13}C NMR spectrum for 2,2-bipyridine-N-oxide (**2a**)

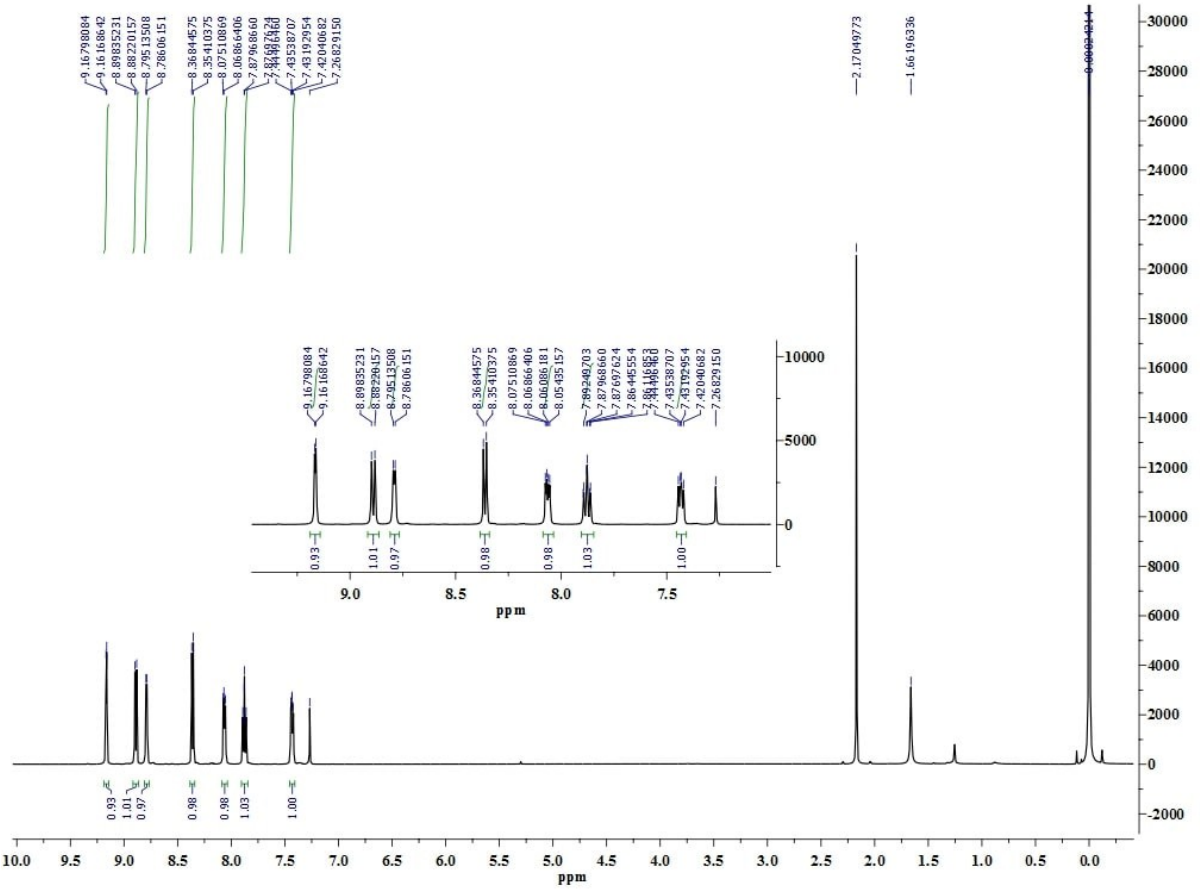

Fig. S5. [1]H NMR spectrum for 4-Nitro-2,2-bipyridine-N-oxide (**2b**)

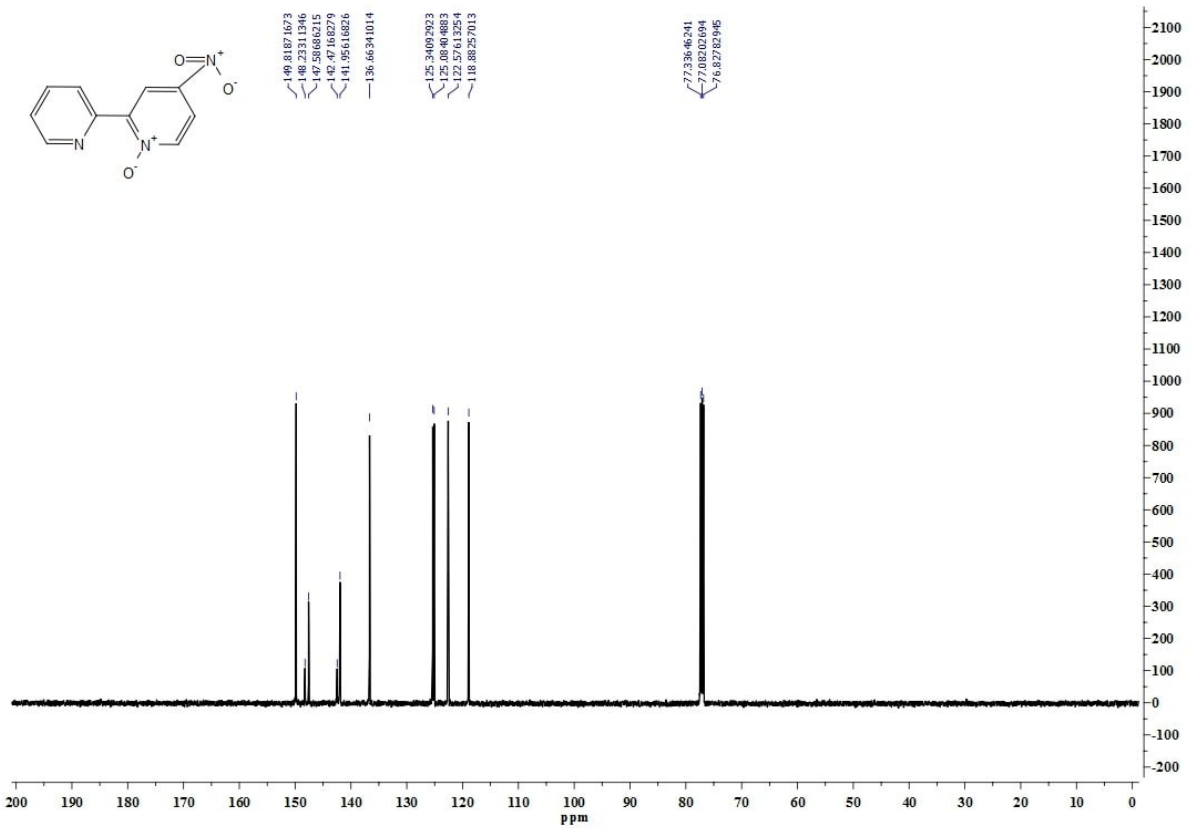

Fig. S6. [13]C NMR spectrum for 4-Nitro-2,2-bipyridine-N-oxide (**2b**)

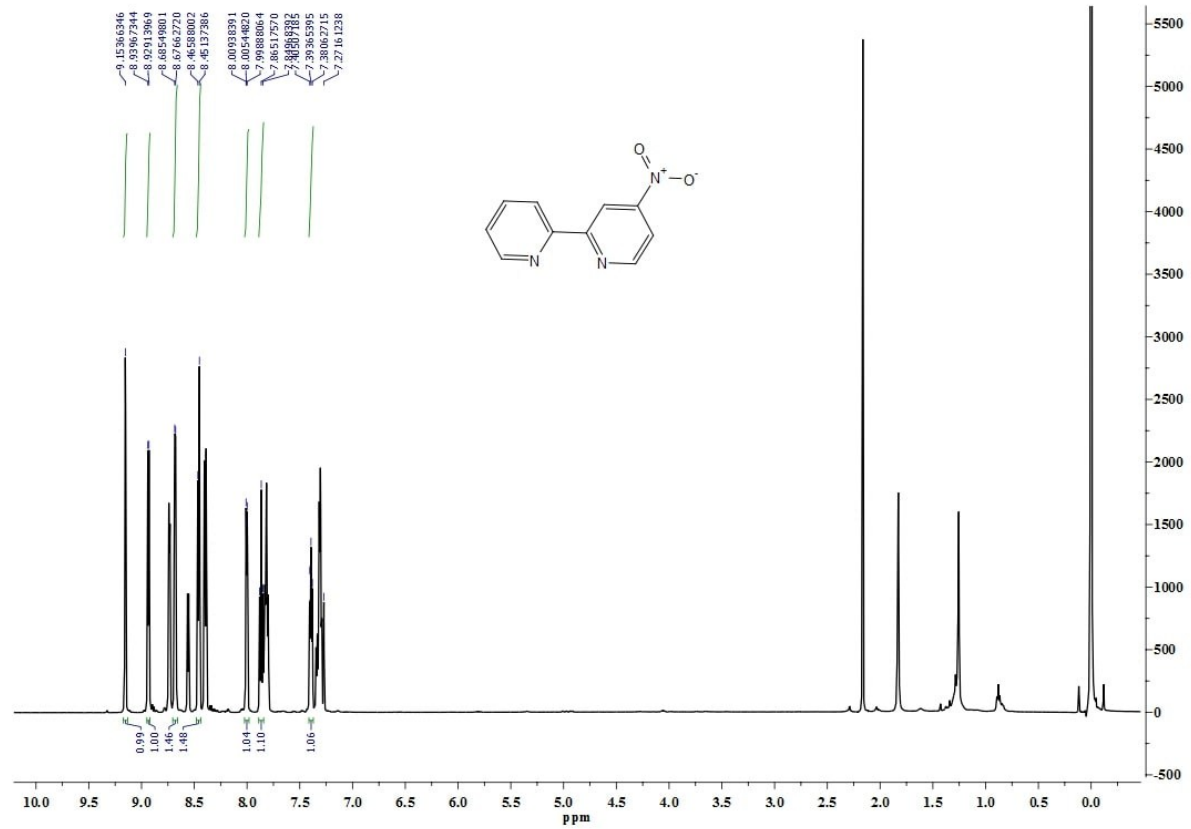

Fig. S7. ^{1}H NMR spectrum for 4-nitro-2,2-bipyridine (**2c**)

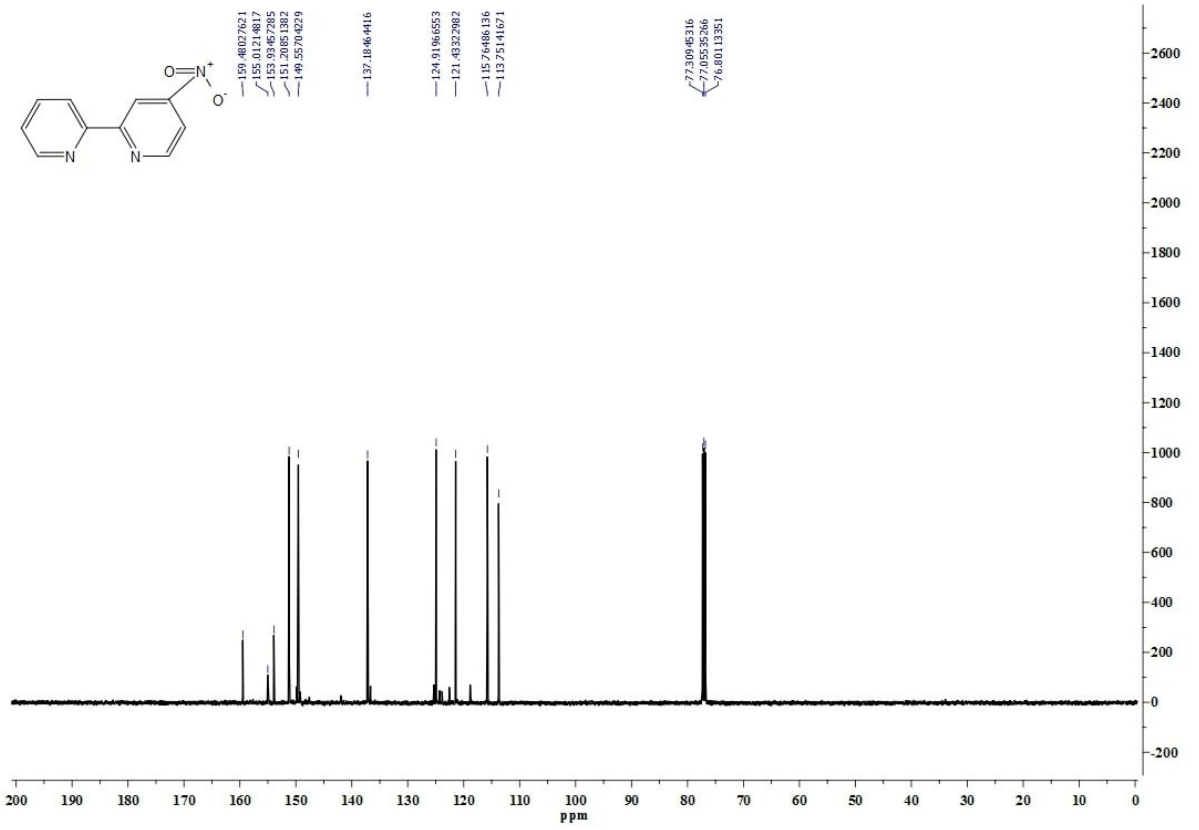

Fig. S8. ^{13}C NMR spectrum for 4-nitro-2,2-bipyridine (**2c**)

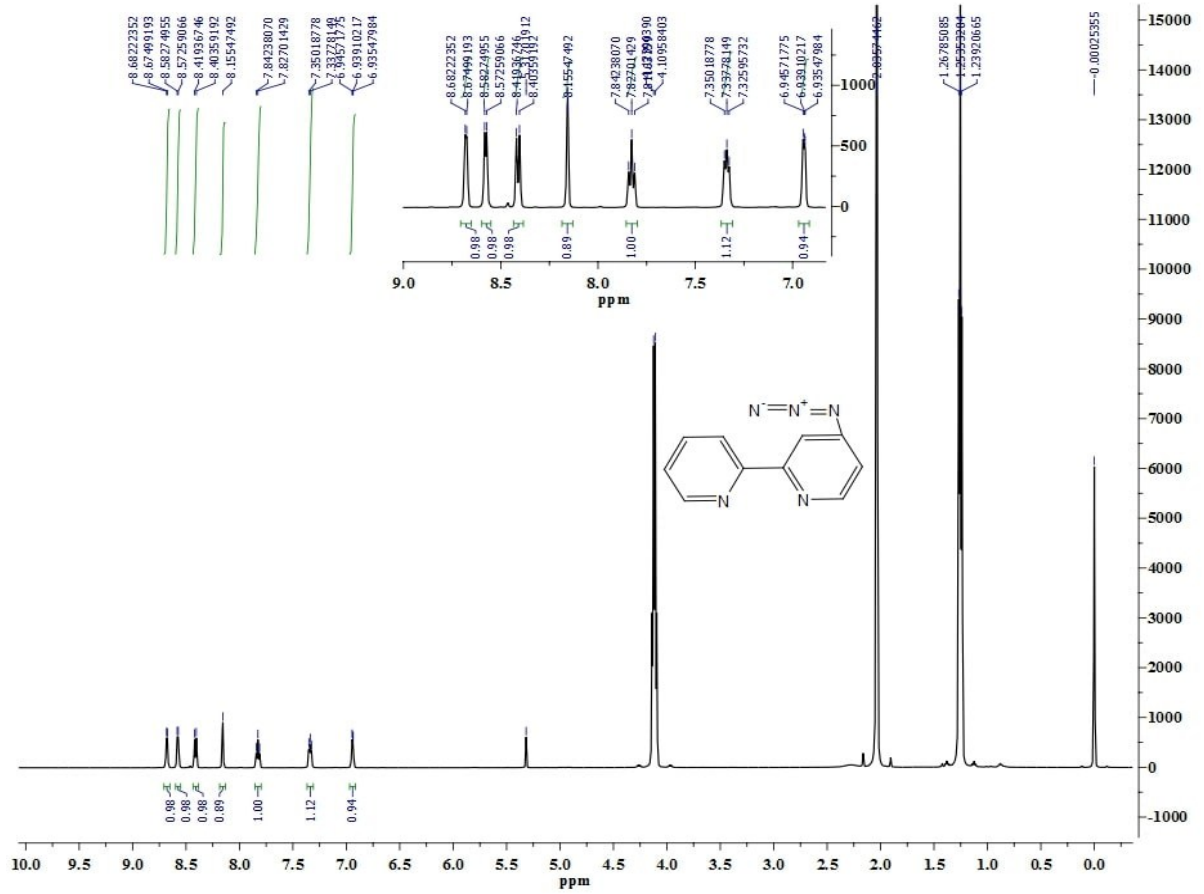

Fig. S9. [1]H NMR spectrum for 4-azido-2,2-bipyridine (**2d**)

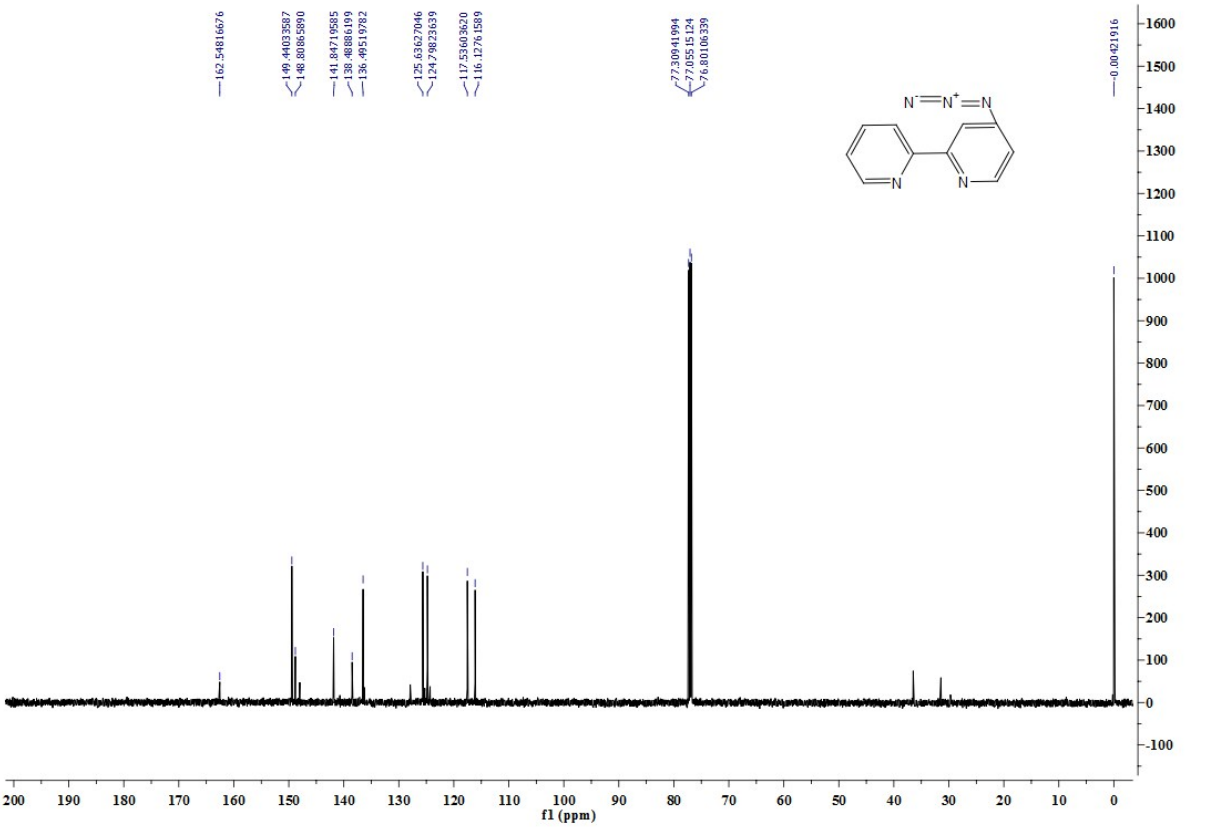

Fig. S10. [13]C NMR spectrum for 4-azido-2,2-bipyridine (**2d**)

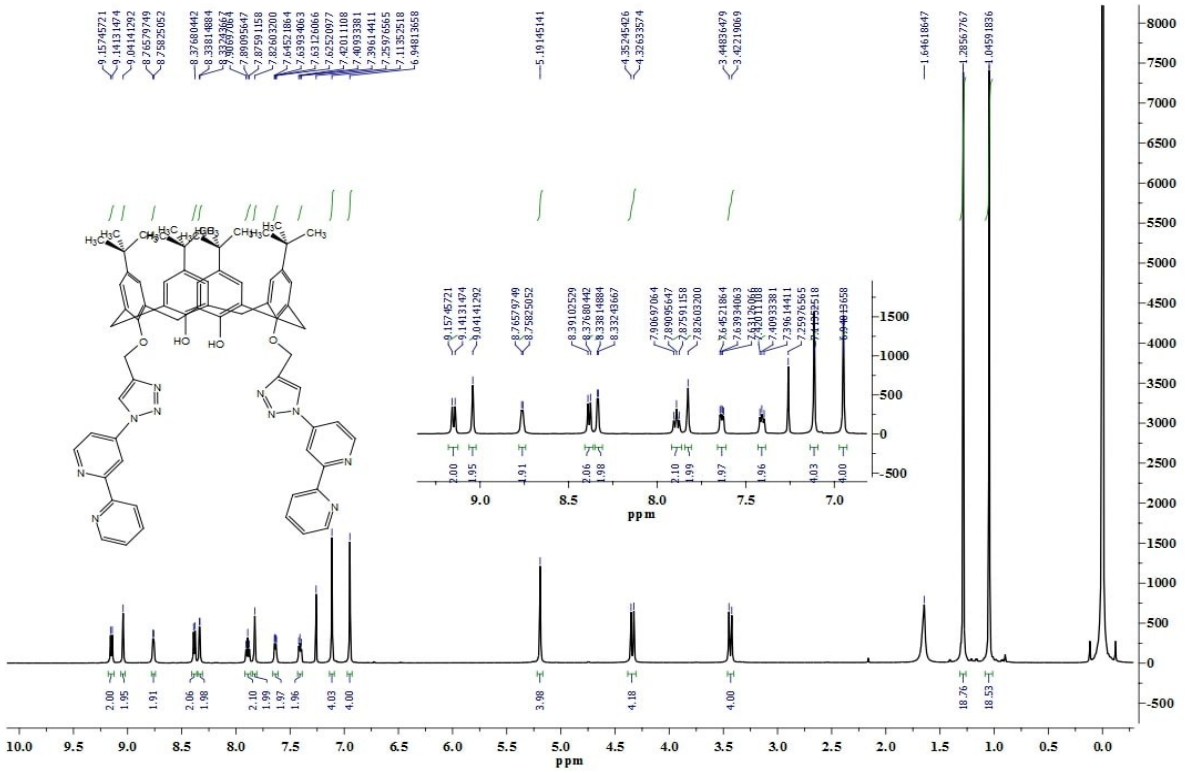

Fig. S11. ^{1}H NMR spectrum for **L**

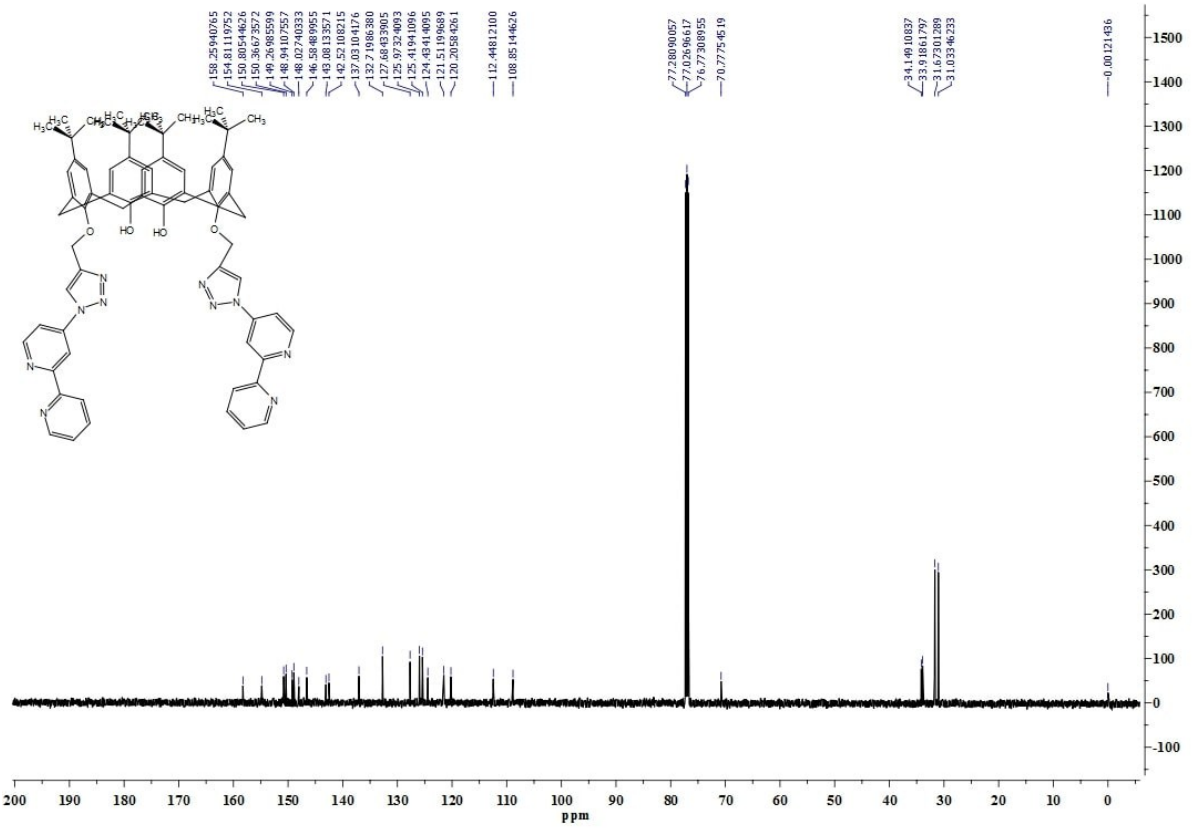

Fig. S12. ^{13}C NMR spectrum for **L**

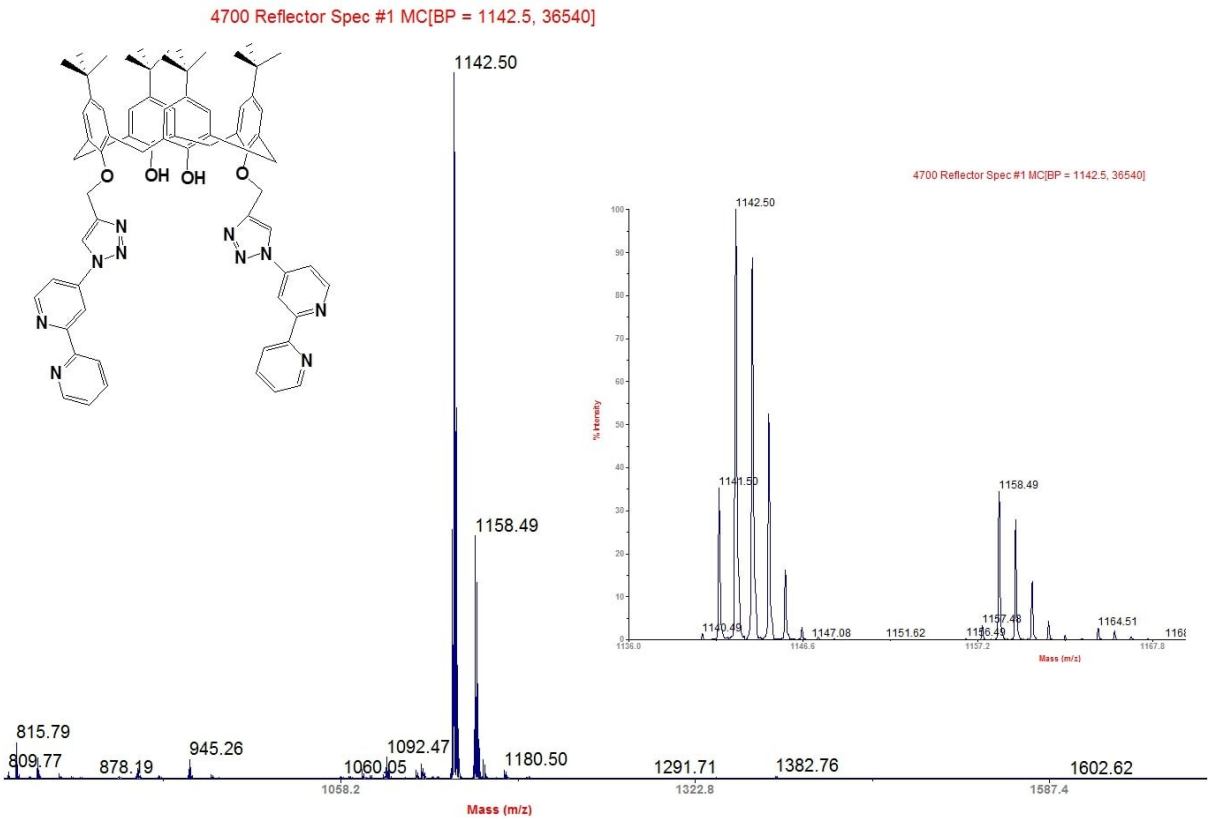

Fig. S13. MALDI-TOF Mass spectrum for **L**

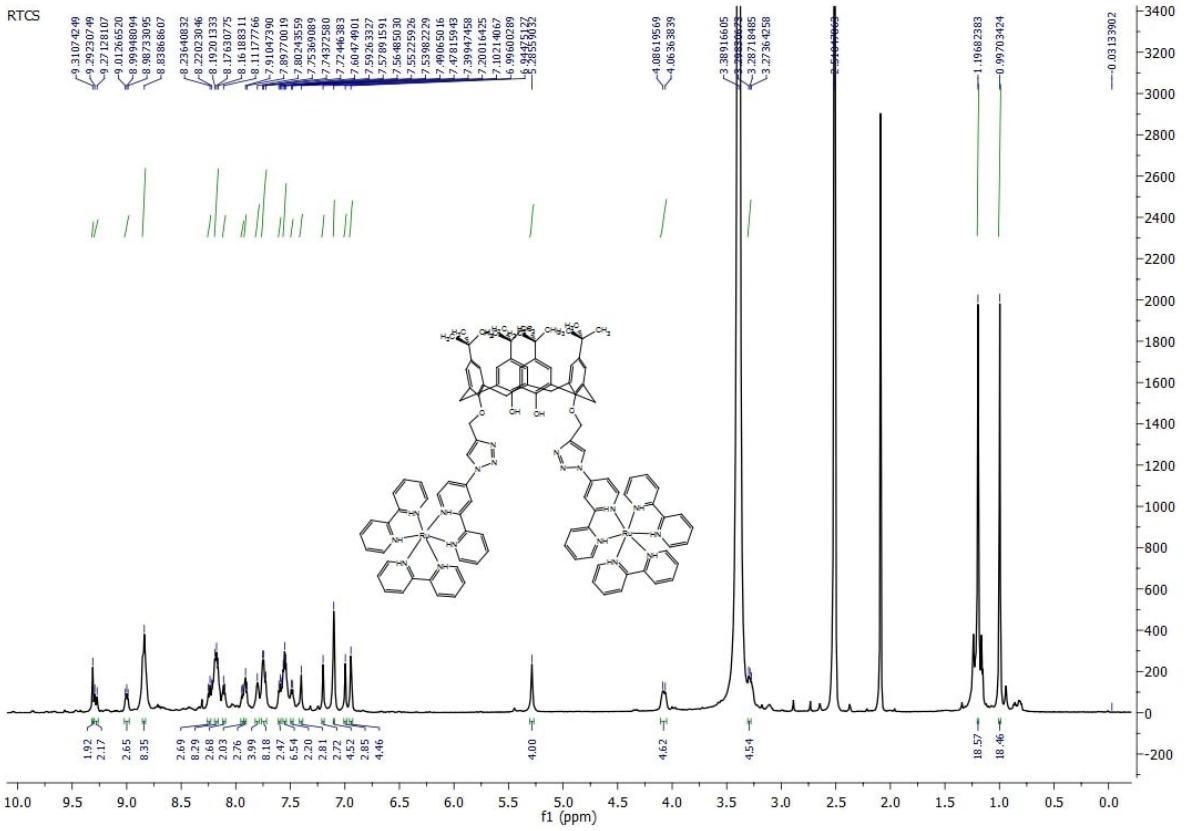

Fig. S14. ^{1}H NMR spectrum for **Ru_2L**

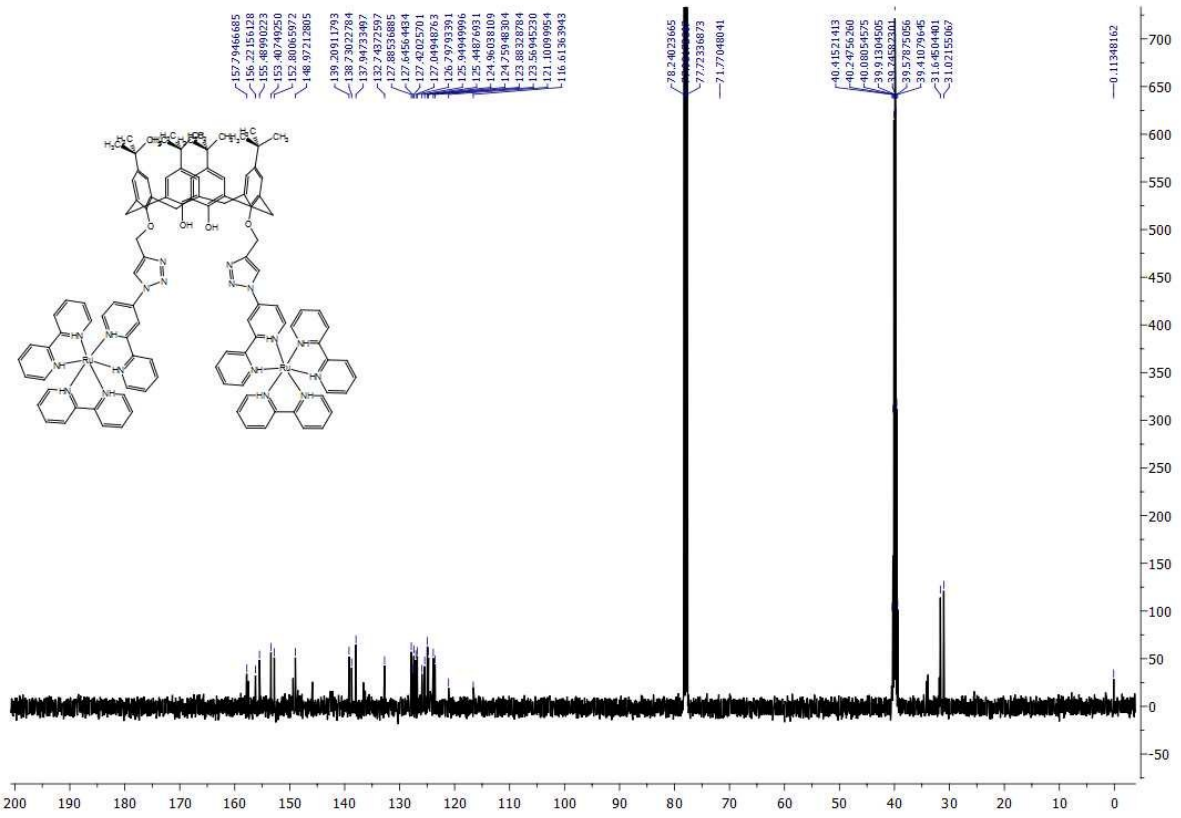

Fig. S15. ^{13}C NMR spectrum for **Ru_2L**

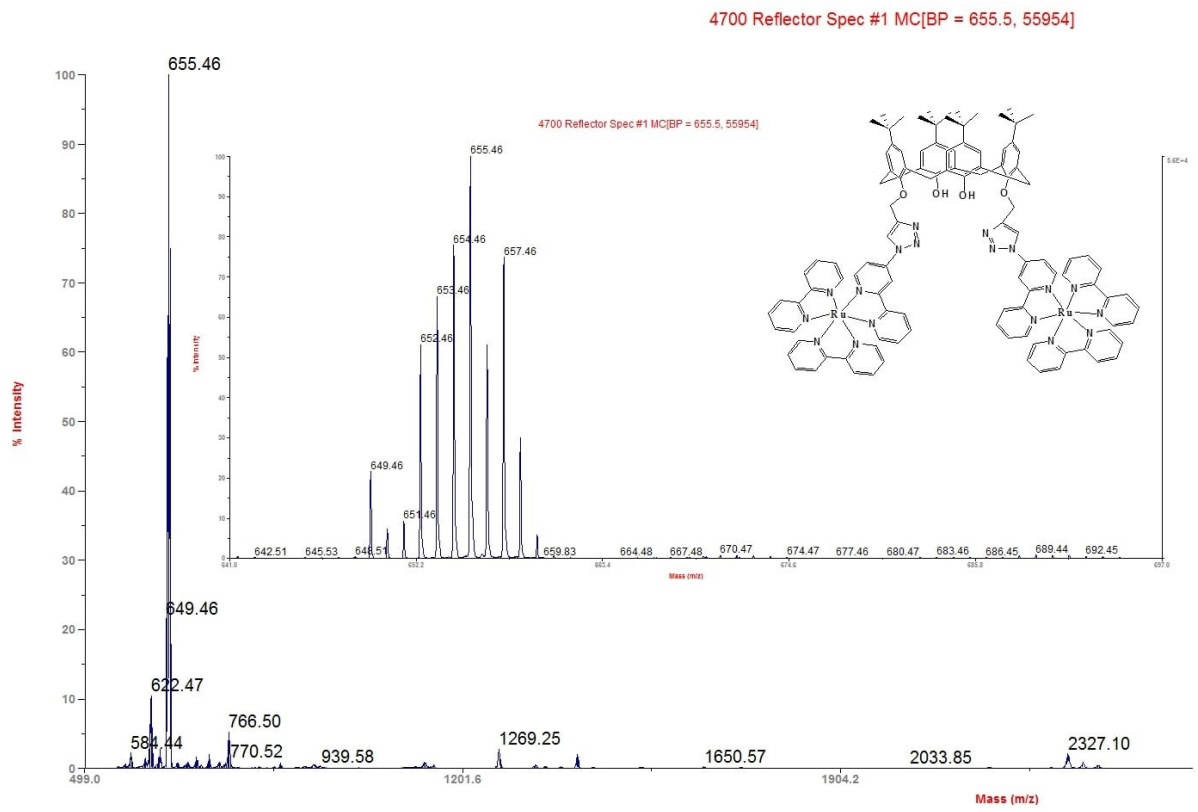

Fig. S16. MALDI-TOF Mass spectrum for **Ru_2L**

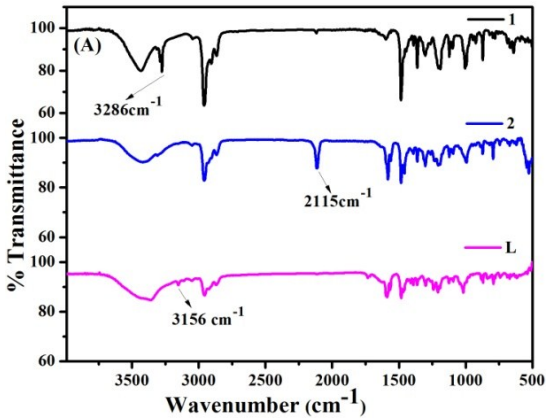

Fig. S17. FT-IR Spectra for Compound **1, 2d** (ATR Mode) and **L**

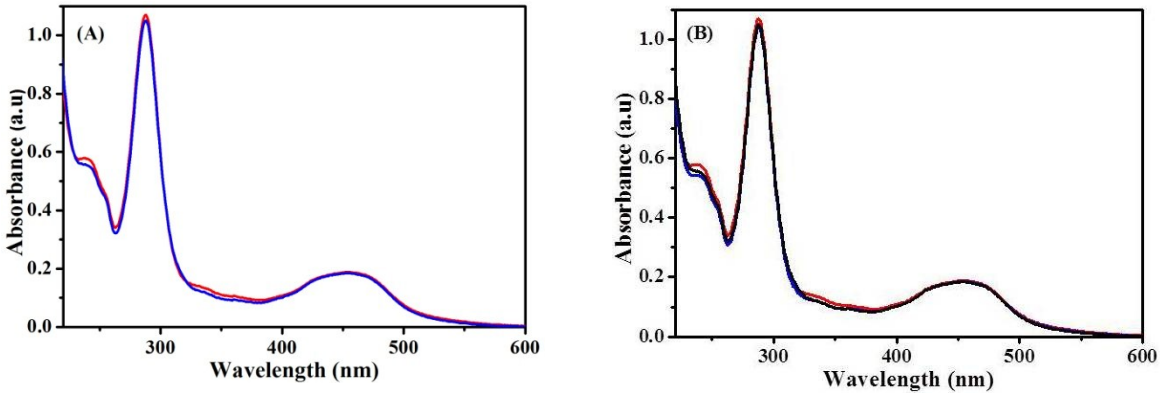

Fig. S18. (A) UV-Vis Spectrum of **Ru_2L, Ru_2L+Various metals ions** (10 equiv.) (blue) **and Ru_2L+Cu^{2+}** (4 equiv.) (red) in 10 μM CH_3CN/HEPES buffer (pH = 7.4) (8/2, v/v) (B) UV-Vis Spectra of **Ru_2L,** + 2 equiv. of Cu^{2+} ion (black) and + 4 equiv. of Cu^{2+} ion (red).

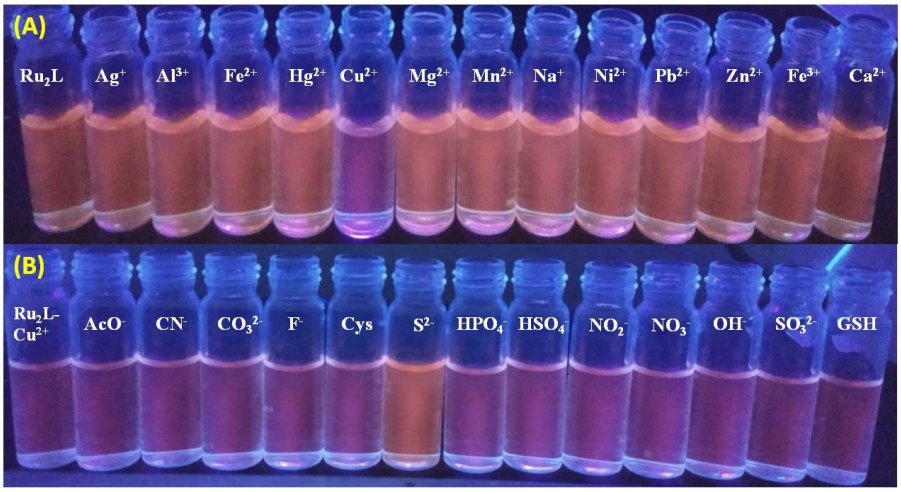

Fig. S19. (A) **Ru_2L, Ru_2L** with various metal ions (B) **Ru_2L-Cu^{2+}, Ru_2L-Cu^{2+}** with different types of anions under UV-light illumination

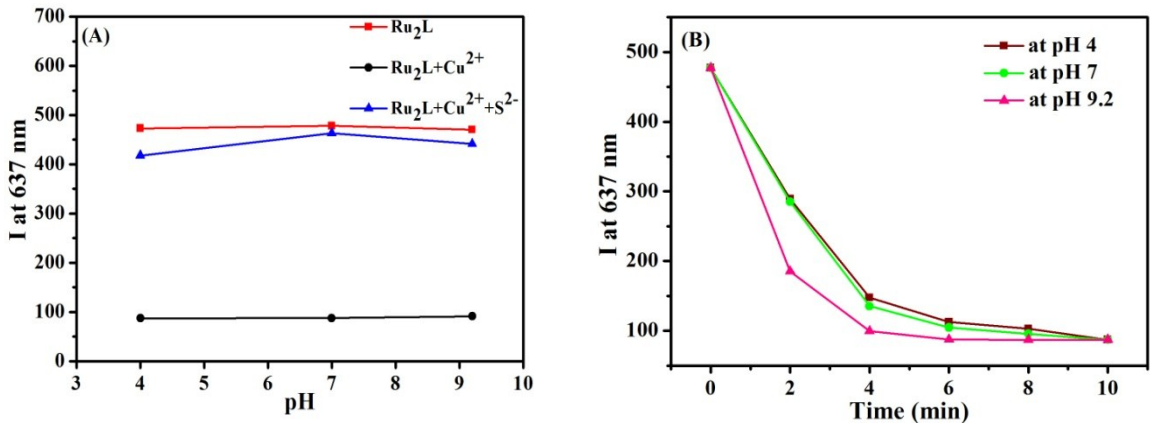

Fig. S20. (A). pH variation was monitored with **Ru_2L**, **Ru_2L-Cu^{2+}** and **Ru_2L-Cu^{2+}+S^{2-}** (B) **Ru_2L-Cu^{2+}** was examined in three different pH values with respect to time.

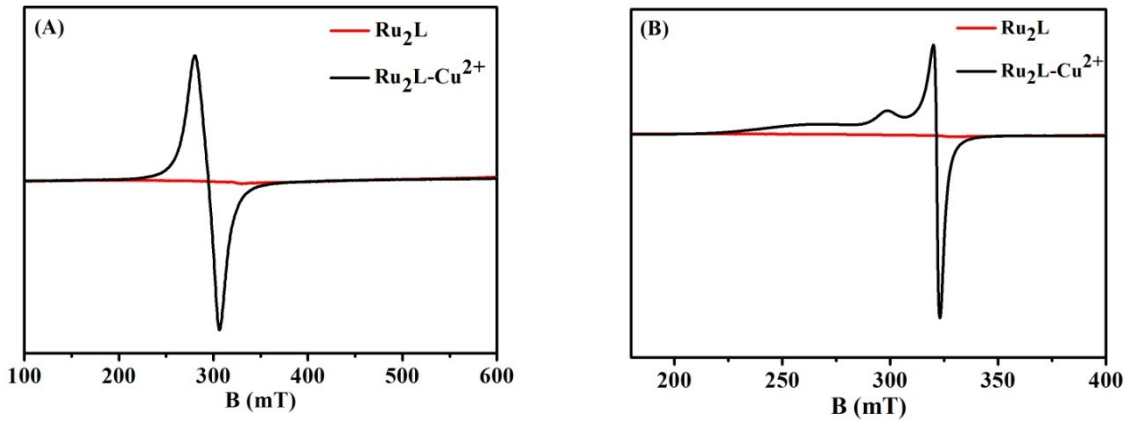

Fig. S21. EPR Spectra of **Ru_2L**, **Ru_2L-Cu^{2+}** at room temperature (A) and liquid nitrogen temperature (B).

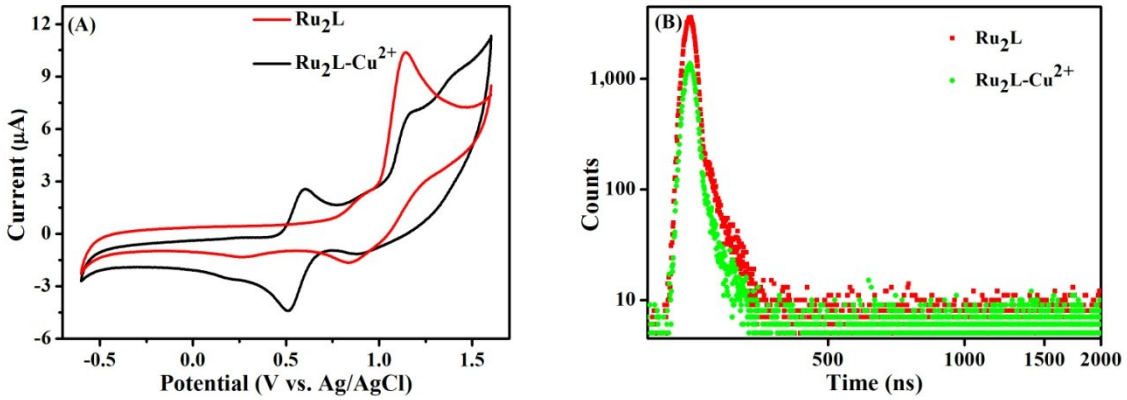

Fig. S22. (A) Cyclic Voltammetric diagram for **Ru_2L** and **Ru_2L-Cu^{2+}**, (B) Time decay profile diagram of **Ru_2L** and **Ru_2L-Cu^{2+}**

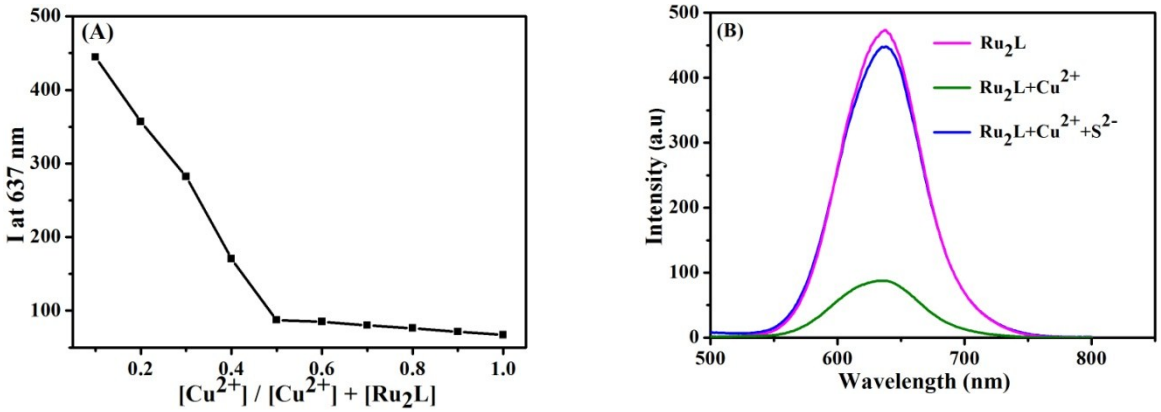

Fig.S23. (A). Job's plot using the fluorescence intensity of **Ru_2L** and Cu^{2+}, (B) **Ru_2L** interaction with Cu^{2+} ion and then S^{2-} anion in CH_3CN/HEPES buffer (pH = 7.4) (8/2, v/v).

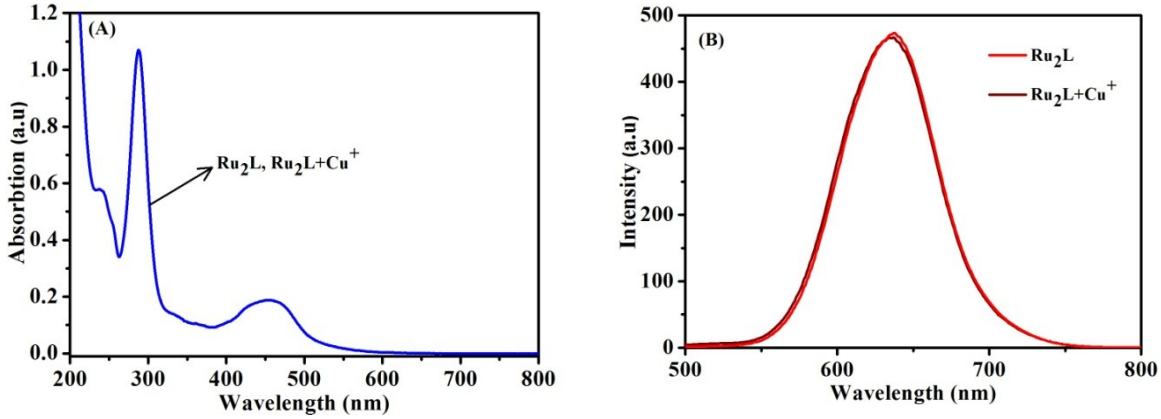

Fig. S24. (A) UV-Vis and (B) Fluorescence spectrum of Ru_2L, Ru_2L+Cu^{+} in 10 μM CH_3CN/HEPES buffer (pH = 7.4) (8/2, v/v)

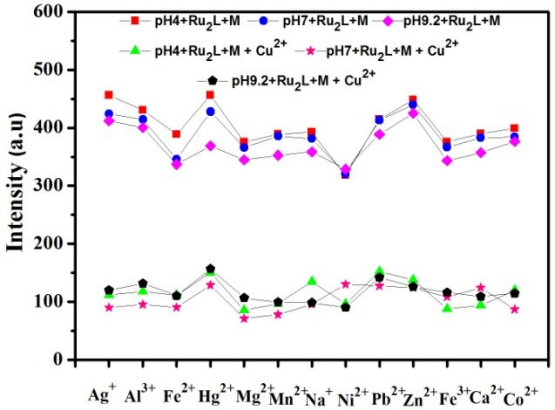

Fig. S25. pH variation was checked to probe with other metal ions (10 equiv.) (Ru_2L+M), in addition of copper (II) ions (4 equiv.) to probe with other metal ions ($Ru_2L+M+Cu^{2+}$) (M = other metal ions).

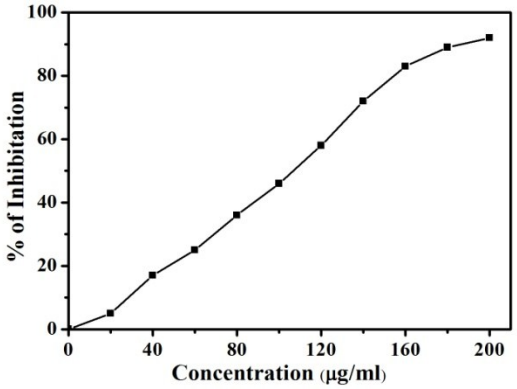

Fig. S26. Cytotoxic effect of the complex **Ru_2L** on A549 cells after exposure for 24 h.

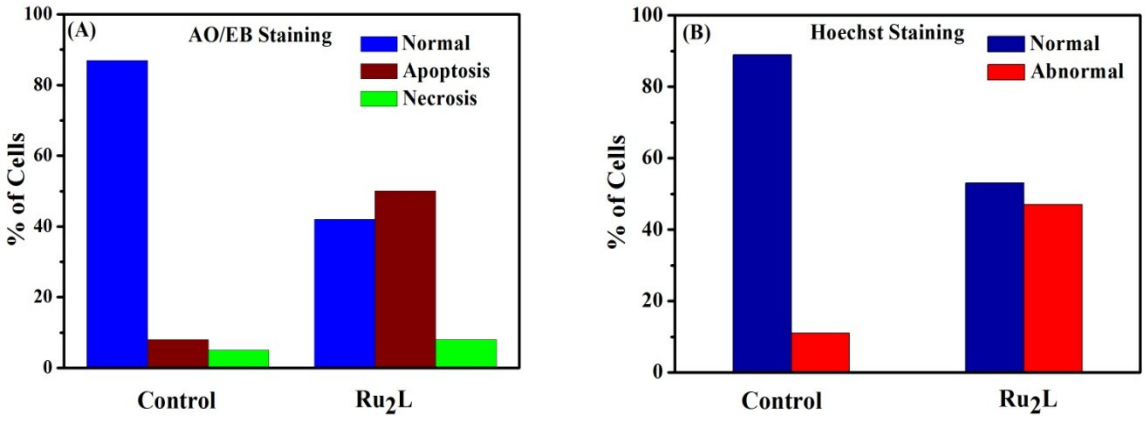

Fig. S27. (A) AO/EB staining indicating the percentage of A549 cells in apoptosis, necrosis and normal cells in control **Ru_2L** treated cells, (B) Hoechst 33258 staining study of control and **Ru_2L** induced apoptosis of A549 cells. The graph is shown a manual count of apoptotic cells in percentage.